INTERNATIONAL JOURNAL OF HYDROGEN ENERGY 45 (2020) 1072–1083

Available online at www.sciencedirect.com

ScienceDirect

journal homepage: www.elsevier.com/locate/he

Flame dynamics analysis of highly hydrogen-enrichment premixed turbulent combustion

*Meng Zhang**, *Min Chang*, *Jinhua Wang*, *Zuohua Huang*

State Key Laboratory of Multiphase Flow in Power Engineering, Xi'an Jiaotong University, Xi'an 710049, China

HIGHLIGHTS

- The highly hydrogen blended turbulent flames were stabilized and measured with laser diagnostic technique.
- Flame topology and characteristics for the lean turbulent combustion and uniform laminar flame speed are investigated.
- Hydrogen effect of high diffusivity on combustion properties is analyzed.
- Hydrogen effect on the local flame front structure is analyzed.

ARTICLE INFO

Article history:
Received 16 April 2019
Received in revised form
2 September 2019
Accepted 25 October 2019
Available online 18 November 2019

Keywords:
Natural gas
Turbulent premixed flames
Hydrogen enrichment
Flame instability

ABSTRACT

The highly hydrogen blended turbulent natural gas flames were stabilized on a nozzle-type Bunsen burner and measured with laser diagnostic technique. Flame topology characteristics and turbulent burning velocities for the lean turbulent combustion and uniform laminar flame speed of $S_L \approx 40$ cm/s were investigated and compared. Hydrogen effect of high diffusivity on combustion properties was analyzed. The local flame structure parameters were obtained and analyzed. Results show that finer wrinkled structure is not only induced by increasing turbulence intensity u'/S_L, but also there is a significant enhancement due to the increasing hydrogen ratio. At large turbulence intensities for lean combustion, more elongated flame folds are formed and small scale structures are generated inducing flame pockets detaching from the main flame, which may largely due to the strong thermo-diffusive effect. However, when fixing $S_L \approx 40$ cm/s, the flame front shows cusp structure with large negative curvature at high hydrogen ratio when u'/S_L is low, which mainly result from Darrieus-Landau instability in influencing the flame-turbulence interaction. Moreover, hydrogen addition apparently enhances turbulent burning velocity and the enhancement is more evident for higher intensities. S_T/S_L seems to follow the power law relation for lean flames while showing a quadratic relation for flame of $S_L \approx 40$ cm/s. The PDF profile widens encompassing a larger range with increasing hydrogen ratio, indicating that the scale of wrinkled structure is getting smaller. This can be further verified by the profile of local radius of curvature. Hydrogen has an evident effect in enhancing flame surface density which may connect to turbulent burning velocity. And a slightly decreasing trend is found when ZH2 is beyond 0.6 at high u'/S_L.

* *Corresponding author.*
E-mail address: mengz8851@xjtu.edu.cn (M. Zhang).
https://doi.org/10.1016/j.ijhydene.2019.10.194

Introduction

The excessive consumption of fossil fuels in the past decades results in the energy crisis, environmental contamination and global warming. Therefore, producing and using the environment friendly alternative fuels are very urgent. Natural gas, mainly composed by methane, is now regarded as a very good transitional fuel, which can not only decrease the dependence on fossil fuels, but also reduce emissions compared to crude oil and coal [1,2]. Even though it has been applied to some combustion devices, i.e. internal combustion engine [3–5], industry and electricity generation [1,6], it is still far from the aim of clean and efficient combustion due to some of its properties, such as low flame propagation speed, poor flammability limits and high combustion instability [7,8]. Hydrogen is regarded as the optimal complementary fuel to methane, due to its large laminar burning velocity. On the other hand, it is perceived as the most renewable energy sources, emits almost zero emission other than water at the point of use [9]. And it has great potential to become large scale common fuel in most combustion device. Therefore, in the fundamental research, natural gas usually burns mixed with hydrogen, which offers many advantages in terms of pollutant reduction, thermal efficiency and combustion stability advancing, allowing some combustion systems to operate with lean fuel mixtures [10]. For instance, investigations show that the thermal efficiency as well as emissions of natural gas engine can be improved by adding hydrogen [3,5,11].

Based on those merits of natural gas with hydrogen on combustion, numerical studies were conducted on this issue. Huang's group [7,12] investigated laminar combustion of natural gas blended with hydrogen and showed that hydrogen affects laminar burning velocity nonlinearly. This can provide basic data for further studies, i.e. the combustion under turbulent conditions. The turbulent burning velocities of methane/hydrogen/air flame and the stretch effect on the flame characteristics were studied [13,14] on combustion chamber and Bunsen burner [15,16]. Results showed that a clear enhancement on turbulent burning velocity is seen with 20% hydrogen for lean mixtures. Indeed, hydrogen effect on methane/air combustion properties, including lean flame instability [11], flame extinction [12] and flame structure [13] were also investigated. The author's group conducted several investigations on flame front characteristics of methane/air with the hydrogen ratio up to 40% [15–17]. To realize the large scale application of hydrogen in future, the turbulent premixed combustion of methane/hydrogen/air in a wide range hydrogen ratio as well as equivalence ratio should be investigated.

Furthermore, turbulent combustion involves both length scale and time scale over a very wide range, i.e. from Kolmogorov scale which is the smallest scale in turbulence to the characteristic scale of the combustor and the chemical reaction time scale to flame propagation time scale. This results in the very complex combustion modes, suggesting turbulent flames at different combustion regimes classified by Peters [18,19]. In normal combustion device, the chemical reaction is very fast comparing to eddy characteristic time scale and confined within a thin layer, leading to a convoluted, local stretched flame structure [20]. The wrinkled structure is the general characteristic of the turbulent premixed flames and mainly resulted from multi scale interaction of flame and turbulence, affected by flame instability in the meantime. Driscoll [20] suggested that the turbulent burning velocity and the parameters of flame front structure, resulted from turbulence-flame interaction, can be used for turbulent combustion modelling and testing the robustness of numerical combustion models. A number of parameters were utilized trying to declare the turbulence-flame interaction, including flame surface density [21,22], local curvature [23], mean flame volume [24] and cutoff scales in fractal theory [25]. Those parameters can also provide very useful data for the guidance on combustor design.

Based on above considerations, the objective of this work is to investigate the detailed flame front structures of methane/hydrogen/air flames, with hydrogen fraction up to 80%. Turbulence in a wide intensity range is generated using a multi-plate strategy and measured by hot-wire anemometer. Instantaneous OH radical profile is detected using planar laser induced fluorescence (PLIF) technique to identify the flame front. The characteristics of hydrogen-enrichment flames and the effects of hydrogen addition are analyzed via the flame front parameters.

Experimental apparatus and methods

The experiments were conducted using a modified multi-plates turbulent premixed Bunsen burner with OH-PLIF technique. The detailed description of experimental setup can be found in Zhang et al. [26]. A brief description is given here. The structure block of the modified multi-plates Bunsen burner is depicted in Fig. 1. The main flame is stabilized at the nozzle with a diameter of 20 mm and surrounded by a co-flame, which can provide a thermo-atmosphere to the main flame and prevent the entrainment of cold ambient air. Cooling water is supplied to keep the nozzle at a proper temperature.

To generate a controllable and more intensive turbulence, the burner, as described in detail in Zhang et al. [16,26], was updated to a multi-plates burner. According to the turbulence theory, a wide-range turbulence (length scales and intensities) can be produced with multi-plates by arranging them in a proper order [27]. As illustrated in Fig. 1 (a), there are four positions, marked as A, B, C and D, where the plates can be installed, such that the plates can be arranged in different order with the steel ring. Each position can be occupied by a steel gasket when no plate is installed. A number of plates in different types were designed in the laboratory, which are not fully described here due to brevity. As a result, we can obtain a controllable turbulence through analyzing the large amount of data set from the multi-plate strategy. Fig. 2 shows the structure of the perforated plates used in this study and its parameters were summarized in.Table 1. The combination of the plates used in the experiment was named by its type and installed position. Taking P3_D as an example, this indicates the plate P3 is installed at D position. Three combinations, P3_D, S2_D, S1_C_S1_D, were used in experiment and the

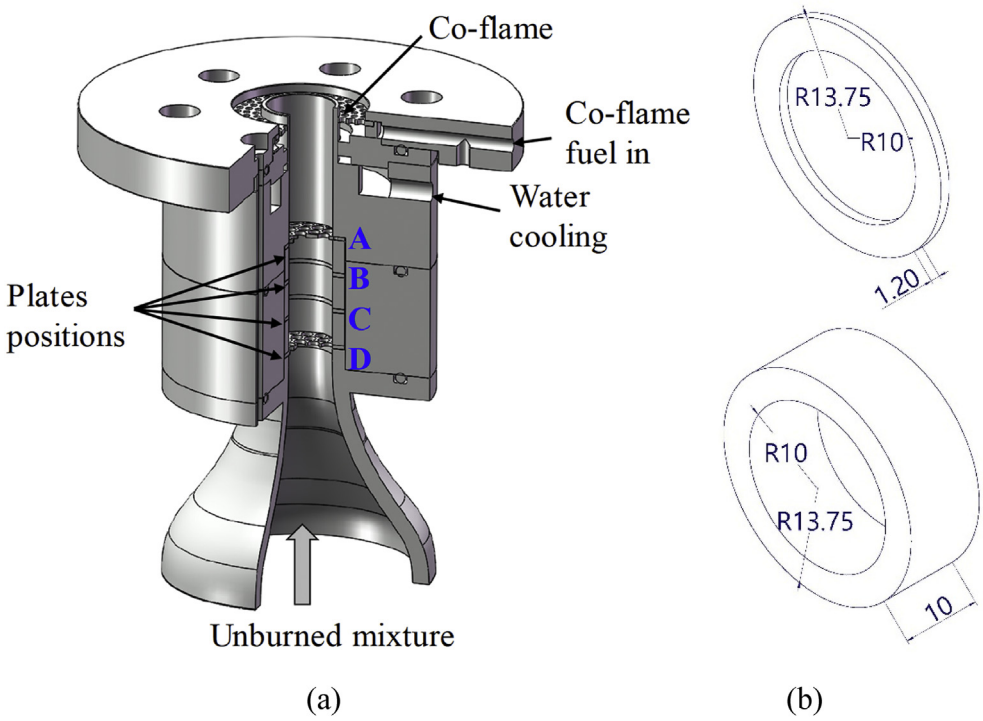

Fig. 1 – (a) Schematic of the turbulent premixed Bunsen burner with multiple plates positions; (b)the rings installed with perforated plates.

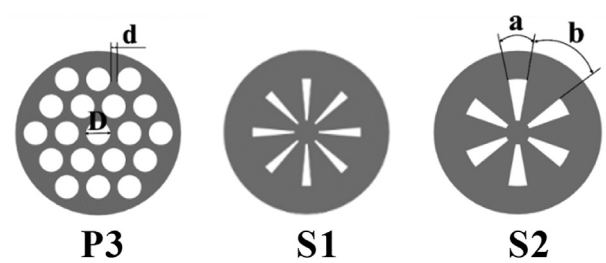

Fig. 2 – Schematic of the perforated plates for turbulence generation.

properties of the generated turbulence will be discussed in detail in the coming section.

Turbulence parameters at outlet were measured with a single hot-wire anemometer (Dantec 55P11) and calculated by Taylor hypothesis and isotropic turbulence assumption as described in our previous studies [16,26]. OH-PLIF measurement system consists of a laser source, ICCD camera (LaVision Image ProX) and the software for signal control and data acquisition. The laser source includes an Nd:YAG laser (Quanta-Ray Pro-190) with a wavelength of 532 nm and a pumped dye laser (Sirah PRSC-G-3000) with a frequency doubler which transfers the wavelength to 282.769 nm. The laser goes through the energy monitor and sheet optics to produce a laser sheet, which is about 50 mm in height and less than 0.5 mm in thickness at the flame position. The OH fluorescence from the (0,0) band at wavelength around 308 nm was detected by an ICCD camera through a UV lens (Nikon Rayfact PF 10545 MF-UV) with intensified Relay Optics (LaVision VC08-0094) and OH bandpass filter (LaVision VZ08-0222).

The hydrogen ratio, ZH2, is defined as ZH2 = XH2/(XCH4 + XH2), where XCH4 and XH2 are the mole fractions of CH4 and H2 in the fuel. ZH2 in the experiment reaches as high as 80%. The laminar burning velocity, S_L, for the mixtures in this study was calculated with the PREMIX code [28] in CHEMKIN-II [29] with GRI-Mech 3.0 [30]. φ represents the equivalence ratio. α_D is the thermal diffusivity of the mixtures and δ_L is the laminar flame thickness calculated by $\delta_L = \alpha_D/S_L$. Effective Lewis number, *Le* was calculated by the volume-based method described in literature [31]. The properties of tested flames are summarized in Table 2.

Table 1 – Parameters of the perforated plates used in this study.

Plate type	P3	Plate type	S1	S2
Open ratio (%)	55.5	Open ratio (%)	17.1	25.7
Number of holes	19	Number of slots	8	6
Diameters D (mm)	4	Open angle a (°)	10	20
Space d (mm)	1.2	Space angle b (°)	35	40
D/d	3.3	a/b	0.3	0.5

Turbulent flow and flame instabilities

Turbulence characteristics

Fig. 3 plots the variation of turbulence intensity *u'* with the mean inlet velocity *U*. It can be seen that *u'* increases linearly with *U* which implies that turbulence intensity is mainly affected by the geometry structure. Thus, the three combination used in the current study can generate wide range

Table 2 – Fuel composition and laminar flame parameters.

ZH2	φ	S_L (cm/s)	α_D (cm^2/s)	δ_L (mm)	*Le*
0	0.60	11.06	0.223	0.202	0.990
	0.80	26.12	0.223	0.086	0.992
	1.00	36.42	0.224	0.062	0.996
	1.20	32.61	0.225	0.069	0.997
0.2	0.60	12.93	0.234	0.181	0.886
	0.96	40.00	0.240	0.060	0.912
0.4	0.60	16.00	0.247	0.191	0.785
	0.70	25.88	0.252	0.118	0.796
	0.85	40.00	0.257	0.064	0.816
	1.00	50.70	0.263	0.063	0.832
	1.10	52.88	0.267	0.062	0.842
	1.20	49.56	0.270	0.069	0.855
0.6	0.60	21.28	0.269	0.127	0.679
	0.75	40.00	0.280	0.070	0.707
0.8	0.60	32.51	0.306	0.094	0.576
	0.65	40.00	0.312	0.078	0.587

intensities. Due to the good linearity, the maximum mean inlet velocity is only up to 7 m/s. We can obtain *u'* at higher inlet velocity through interpolation. The integral length scale l_0, which represents the mean size of the energy bearing vortex, and Kolmogorov scale l_K, corresponding to the smallest scale in turbulence, with respect to turbulence intensity *u'* are also plotted in Fig. 4. The results show that l_0 decreases with *u'* for P3_D while it almost keeps constant value for S2_D and S1_C_S1_A, though the scatter is seen for S1_C_S1_A. This implies that we can obtain different turbulence intensities at the same integral scale. When looking at Kolmogorov scale l_K, all the measured data collapse to a common curve, which indicates that the smallest scale in turbulence is only related to the fluctuations of the velocity field. Those curves are regarded as the properties of the plates.

Laminar flame speed

The laminar flame speed S_L with hydrogen ratio in current study was plotted in Fig. 5. It can be seen that S_L increases significantly with hydrogen ratio due to the high reactivity of H_2. There exists a maximum value of S_L-φ relation for both

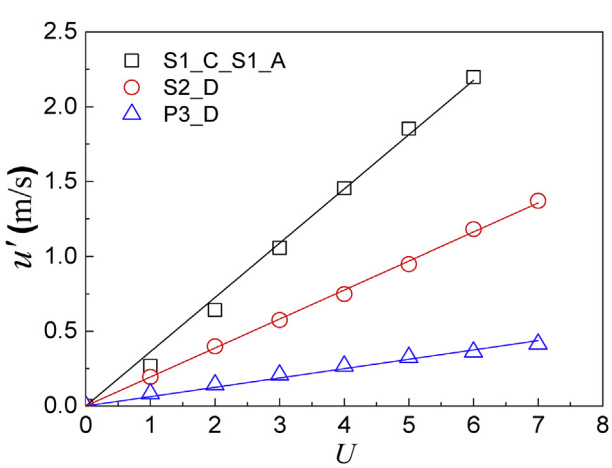

Fig. 3 – dependence of the turbulence intensity *u'* upon mean inlet velocity *U*.

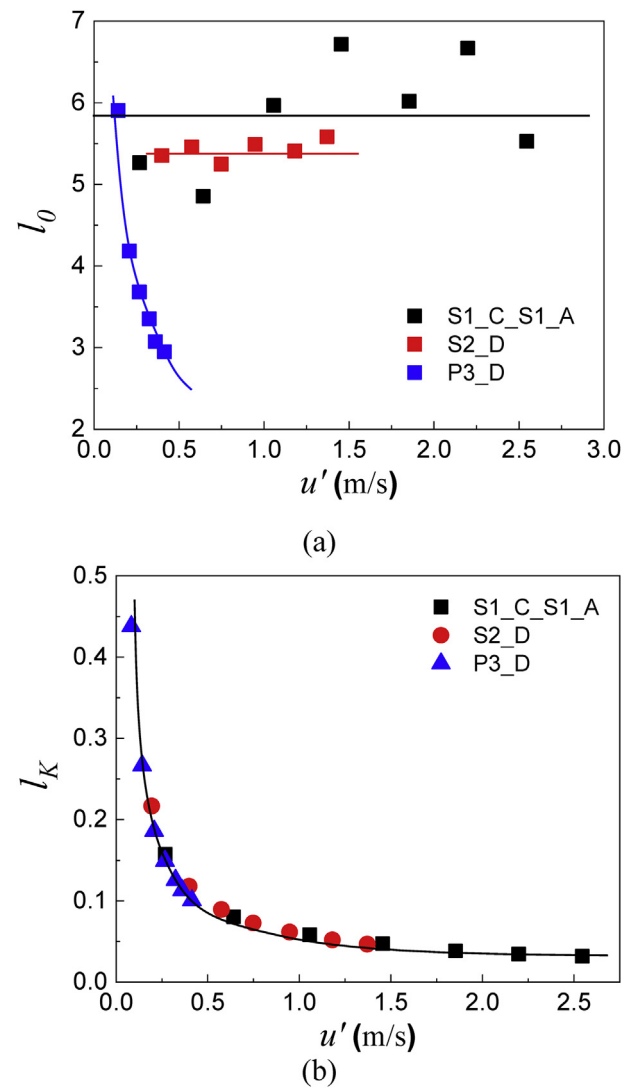

Fig. 4 – Variation of the (a) integral scale (l_0) (b) Kolmogorov scale (l_K) with turbulence intensity (*u'*).

pure methane and hydrogen, the corresponding φ is 1.1 and 3.0 respectively. Thus, we can see that S_L for $\varphi = 1.2$ is larger than that of $\varphi = 1.0$ at ZH2 = 0, while S_L for $\varphi = 1.2$ is smaller than that of $\varphi = 1.0$ at ZH2 = 0.8. For ZH2 larger than 0.4, S_L increases monotonically with equivalence ratio, which indicates that S_L is dominated by the property of H_2. The laminar flame speed is the property for the fuel which can be used as a basic parameter to analysis the local flame speed of the turbulent flame and to normalize the turbulent burning velocity.

Results and discussions

The tested turbulent flames in Borghi's diagram were depicted in Fig. 6 [18]. Most flames locate in the flamelet regime and also some flames locate in thin reaction regime. As a consequence, the flame front can be treated as a thin layer which can be identified by the sharp increase of the OH radical

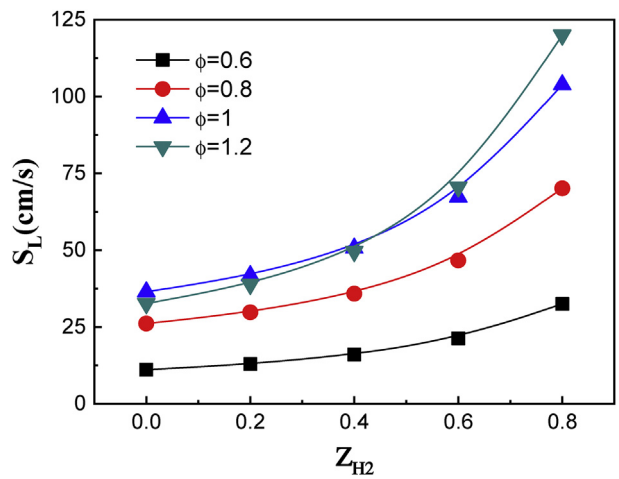

Fig. 5 – Variation of laminar flame speed with equivalence ratio (φ) and H_2 blending ratio (Z_{H2}).

distribution during the combustion [15,26]. The turbulent flame parameters are obtained by image processing method developed by Zhang et al. [16,32].

Hydrogen ratio effect on lean combustion

Firstly, lean turbulent combustion was investigated. The typical OH-PLIF snapshots of turbulent premixed flames for ZH2 from 0 to 0.8 at $\varphi = 0.6$ was given in Fig. 7. Due to brevity, only three hydrogen ratios were shown and full images were provided in the supplementary material. To stabilize the flame at high hydrogen ratio, the bulk inlet velocity U_{ave} was adjusted. To facilitate the discussion, the U_{ave} and turbulence intensity u' of each case were indicated in Fig. 7. There were two bulk inlet velocities in experiments and the turbulence data were also provided in Table 3. We see that finer wrinkled structure is not only induced by increasing turbulence intensity, but also there is a significant enhancement due to the increasing hydrogen ratio. As the turbulence perturbation is increased, more large scale elongated flame folds are formed and imposed by small scale structures, inducing flame pockets detaching from the main flame, as depicted in Fig. 7. Moreover, the flame height, which is a representation of flame residence time in a jet flame, decreases with turbulent intensity and hydrogen ratio. This indicates that fuel properties can highly affect the combustion performance.

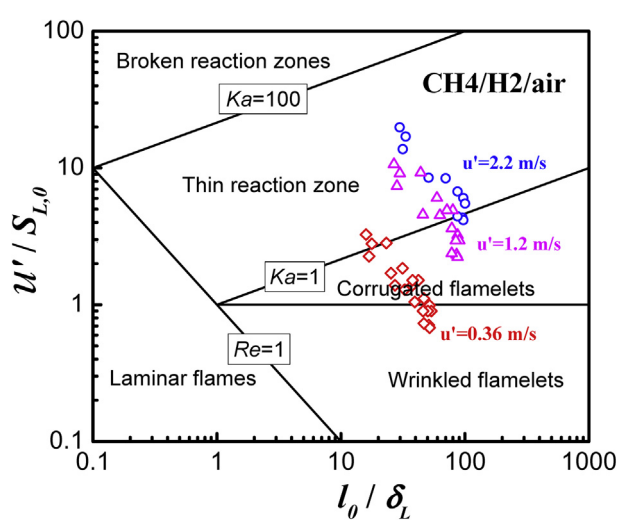

Fig. 6 – Experimental data sets in Peters-Borghi's diagram.

To clarify hydrogen ratio effect on the global property of the turbulent premixed flames, the variation of turbulent burning velocity S_T/S_L with ZH2 is shown in Fig. 8. S_T is calculated by the angle method $S_T = U\sin(\theta/2)$, where θ is the cone angle derived from flame leading edge and U denotes the bulk inlet velocity. U was kept at 6 m/s for most cases and was adjusted to 10 m/s for large turbulence intensities at high ZH2 to prevent flash back due to the larger S_L as designated in Fig. 5. Also, the normalized turbulent intensities u'/S_L for each cases are listed. The three curves show the variation of turbulent burning velocity S_T/S_L with hydrogen ratio ZH_2 at low, medium and high turbulence intensities. Therefore, Fig. 8 illustrates a solely hydrogen effect, which also mentioned as fuel effect in the literature [33]. It is clearly seen that hydrogen addition can enhance S_T/S_L and the enhancement is more evident for higher intensities, which shows a consistent behavior when hydrogen ratio is below 0.2 [15]. Moreover, the increase of S_T/S_L is sharper at low hydrogen ratio and then seems to show a flat trend, which seems to follow a power law. Since the flamelet concept was assumed in current study, the increase of turbulent burning velocity is due to 1) increase of flame front area caused by the turbulence perturbation, 2) the laminar flame properties, such as Lewis number effect. Firstly, as the increasing of u'/S_L, small scale flame front is the dominate structure, leading to finer wrinkles or larger flame front area and consequently increase the burning velocity. Then hydrogen addition modifies the preferential diffusion, especially for large hydrogen ratio, leading to a larger thermal diffusive effect on local flame front, which will be further analyzed.

In lean combustion, fuel is insufficient and the local chemical reaction within flame largely depend on the local fuel concentration. For simplicity, the flame instability analysis is based on a quasi-steady curved flamelet model as illustrated in Fig. 9. Here we assume a mixture that has faster molecular diffusion of reactants, namely $Le < 1$. When the flame is convex towards the unburned region as depicted in Fig. 9(a), due to the faster molecular diffusion to unburned gas, the cold reactants diffuse to a limited zone and are heated, resulting the local fuel concentration increasing and burning faster. As a consequence, local flame speed becomes larger than the unstreched laminar flame speed, namely $S_{L,k} > S_L$. The local flamelet will intrude into unburned region longer. While for the concave structure, reactants diffuse in a large zone resulting $S_{L,k} < S_L$. The local flamelet will drag the main flame forming long flame folds and unburned pockets. This situation is thermos-diffusive unstable and the wrinkling increases leading to larger flame surface area as well as turbulent burning velocity. On the other hand, the Darrieus-Landau Instability (DL instability) resulted from gas expansion also has great effect on flame propagation under flamelet concept. Fig. 9(b) illustrates the flame surface affected by DL instability as propagating downwards. Due to the large density variation across the flame, a highly pointed crests (cusps) structure intruding into burned gas and wide rounded troughs convex

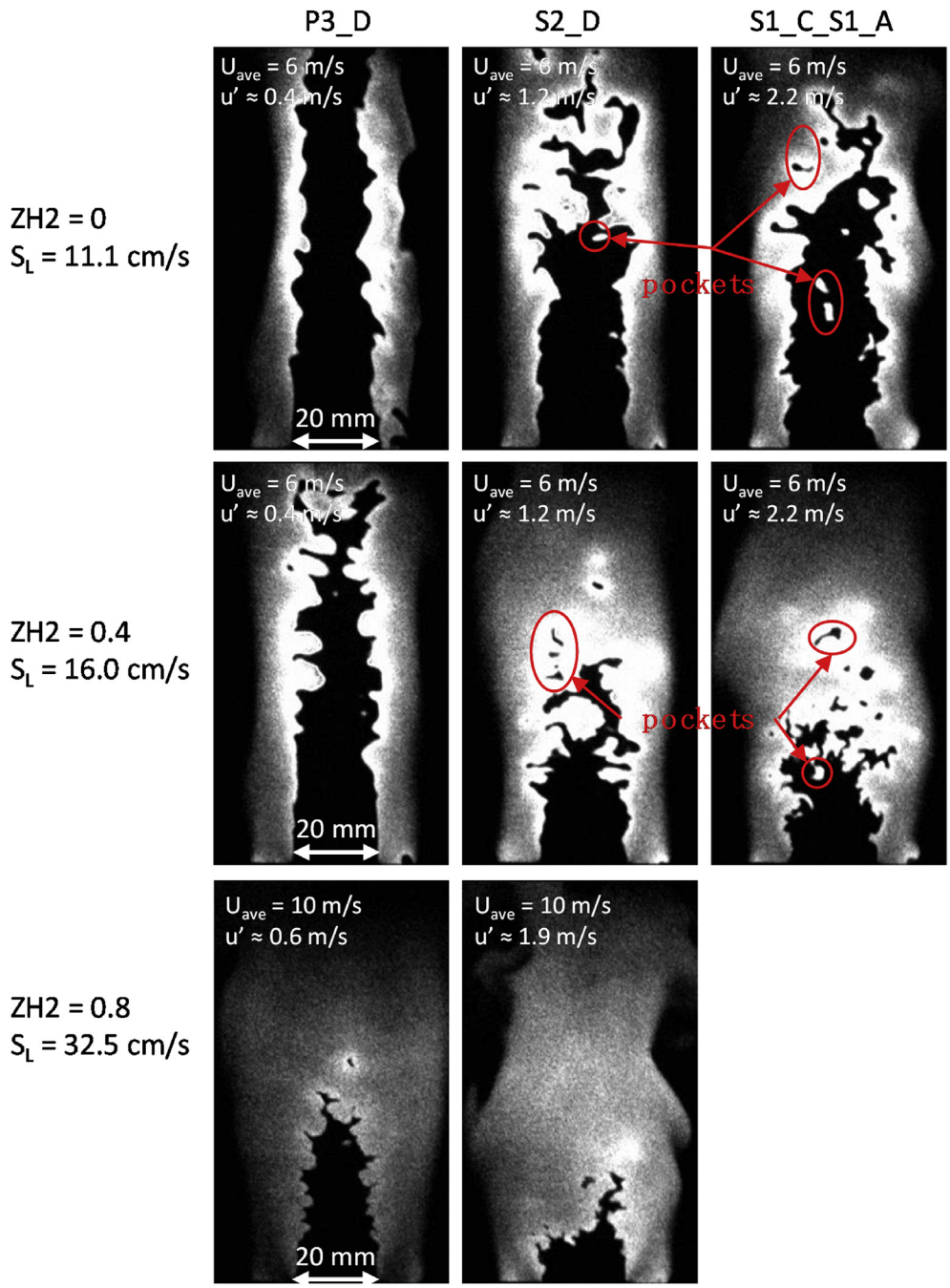

Fig. 7 – Hydrogen ratio effect on flame front characteristics of the turbulent premixed flames of $\varphi = 0.6$.

to unburned gas is formed [34,35]. This would also cause larger local flame speed and flame surface area.

Thus, turbulent flames at fuel lean condition are highly affected by thermos-diffusive instability. It can be also seen that *Le* decreased significantly with higher hydrogen ratio in Table 2, i.e *Le* = 0.99 for ZH2 = 0 and *Le* = 0.58 for ZH2 = 0.8. This indicates thermos-diffusive effect is strengthened with hydrogen ratio and further clarify that the flame is more wrinkled and more flame pockets are formed with higher hydrogen ratio.

Table 3 – Turbulence characteristics.

Plate type	u' (m/s)	U_{ave} (m/s)	Q_R (L/min)	l_0 (mm)	l_λ (mm)	l_K (mm)
P3_D	0.361	6.0	113.10	3.073	0.362	0.113
	0.565	10.0	188.50			
S2_D	1.181	6.0	113.10	5.408	0.261	0.052
	1.955	10.0	188.50			
S1_C_S1_A	2.198	6.0	113.10	6.670	0.212	0.035

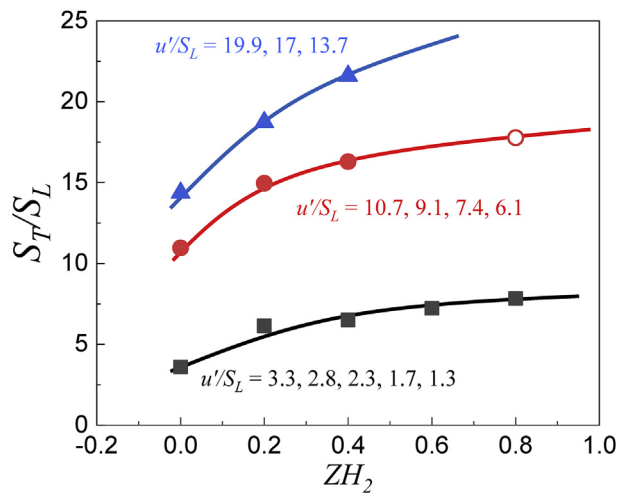

Fig. 8 – Effect of hydrogen ratio effect on turbulent burning velocity for lean turbulent combustion at $\varphi = 0.6$. The bulk inlet velocities are kept at 6 m/s for the solid symbols and 10 m/s for open symbols.

Hydrogen ratio effect on uniform laminar flame speed

To compare with the flames at fuel lean condition in Fig. 8, we investigated the hydrogen ratio on turbulent flames while keeping $S_L \approx 40$ cm/s by adjusting the equivalence ratio. The typical OH-PLIF images are shown in Fig. 10. As discussed earlier, all flames possess convoluted flame front. The flame front tends to be much finer and more wrinkled with the increase of turbulence intensity and hydrogen fraction. In particular, compared with images of $\varphi = 0.6$, those images show cusps on the flame surface of high negative curvature, defined as the structure convex to reactants, at high hydrogen ratio when u'/S_L is low, as pointed in Fig. 10. The cusp is a typical structure resulting from DL instability, indicating that DL instability may play a major role in influencing the flame-turbulence interaction in the flame of high hydrogen ratio, i.e. ZH2 = 0.6 and 0.8. When looking at turbulent burning velocity in Fig. 11, showing a similar trend as Fig. 8, namely hydrogen addition can result in larger S_T/S_L and the enhancement is more evident at higher intensities. However, the difference is that S_T/S_L seems to show a quadratic relation with u'/S_L in Fig. 11 while a power law is seen in Fig. 8. This implies that hydrogen show different S_T behavior when applying for different combustion strategy.

Local flame front characteristics

Since turbulent burning velocity is a global parameter and the analysis on the typical OH-PLIF flame image is fairly qualitative, more detailed information is needed to characterize the combustion properties. PDF distribution of flame curvature and the radius of curvature are usually used to indicate the wrinkled flame front structure [8,9]. For each case, instantaneous flame location was firstly extracted from OH-PLIF image, as illustrated in Fig. 12 (a). Then the pixels along the flame surface are ordered with a proper step. A function describing the flame was obtained by fitting the ordered points with the cubic spline interpolation, as depicted in Fig. 12 (b).

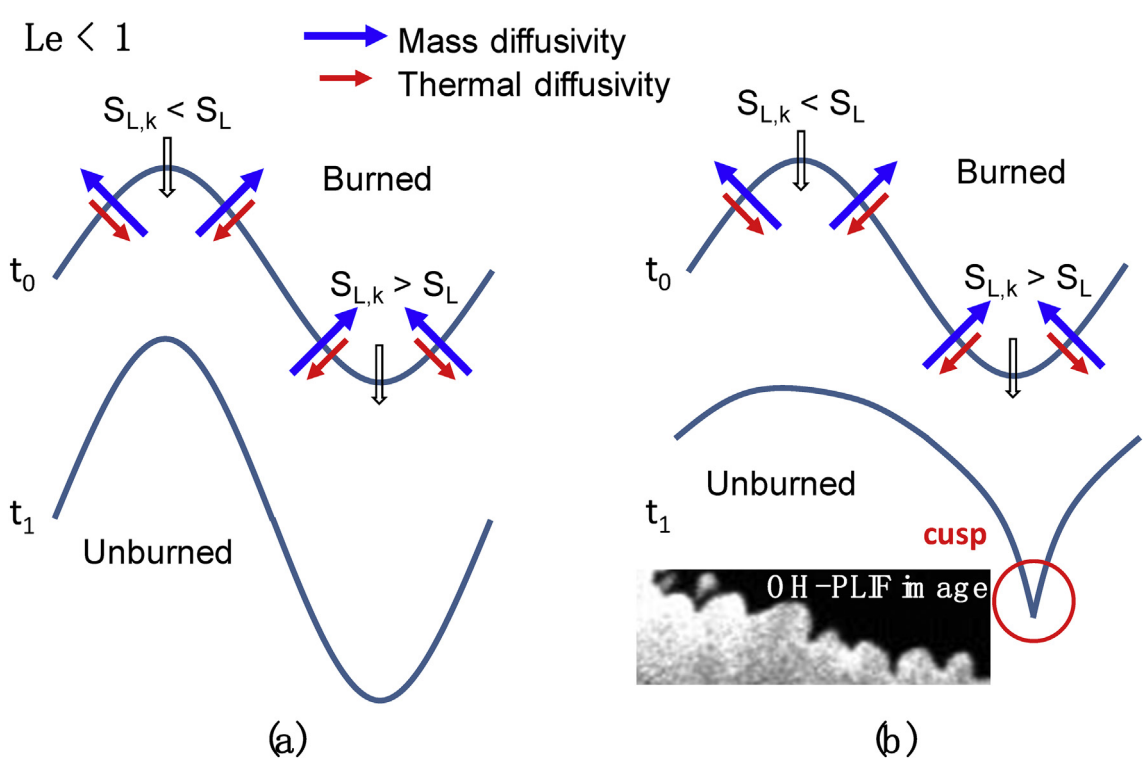

Fig. 9 – Sketch of flame instabilities based on a flamelet model. The flame propagates downwards. (a) thermos-diffusive instability, for *Le* < 1, molecular diffuses (long blue arrows) faster than heat (short red arrows) leading to a larger flame front surface; (b) Darrieus-Landau instability induced cusp. (For interpretation of the references to colour in this figure legend, the reader is referred to the Web version of this article.)

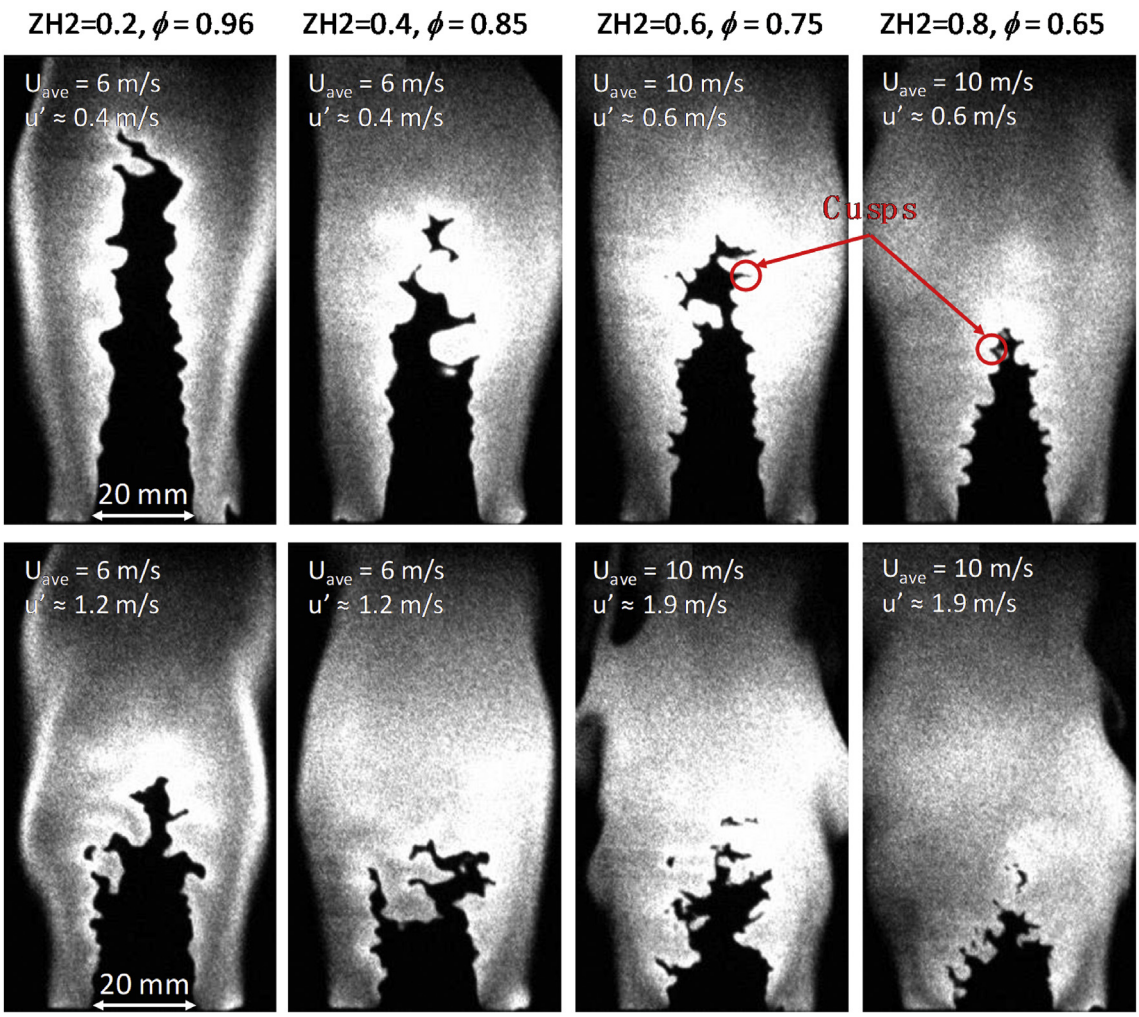

Fig. 10 – Flame front characteristics for SL ≈ 40 cm/s at different ZH2 at low and high turbulent intensities. The perforated plates used are: P3_D for upper panel and S2_D for lower panel.

Once the spline function was obtained, the curvature and the radius of curvature can be calculated by the first and second derivatives as follows,

$$\kappa = \frac{x'(s)y''(s) - y'(s)x''(s)}{(x'(s) + y'(s))^{3/2}} \tag{1}$$

$$r = k^{-1} \tag{2}$$

where $x(s)$ and $y(s)$ are the function with respect to the arc length of the flame s. $x'(s)$ and $x''(s)$ denote the first and second derivatives of function $x(s)$ respecting to s, so do $y'(s)$ and $y''(s)$. It is worth to note that the step of fitting should not be too small, which would cause noise due to limited resolution, or too large, which would not capture the small scale structure. Moreover, according the definition, the structure convex to unburned gas is positive, otherwise is negative. Since the effect of hydrogen addition on the trend are pretty the same, only data of uniform laminar flame speed, namely $S_L \approx 40$ cm/s, are presented in this study.

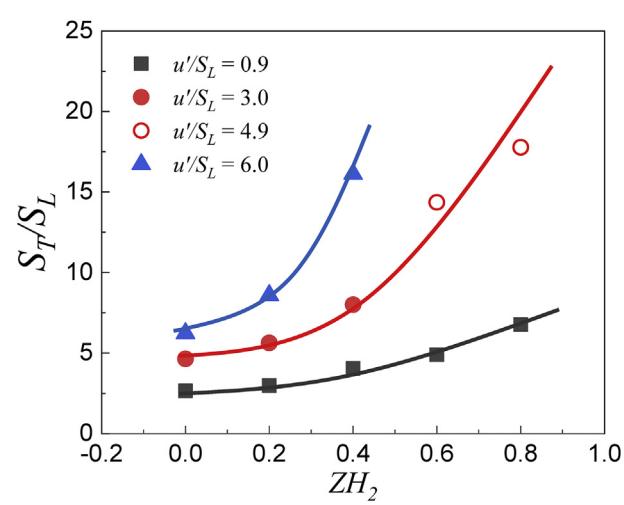

Fig. 11 – Effect of hydrogen ratio effect on turbulent burning velocity for SL ≈ 40 cm/s The bulk inlet velocities are kept at 6 m/s for the solid symbols and 10 m/s for open symbols.

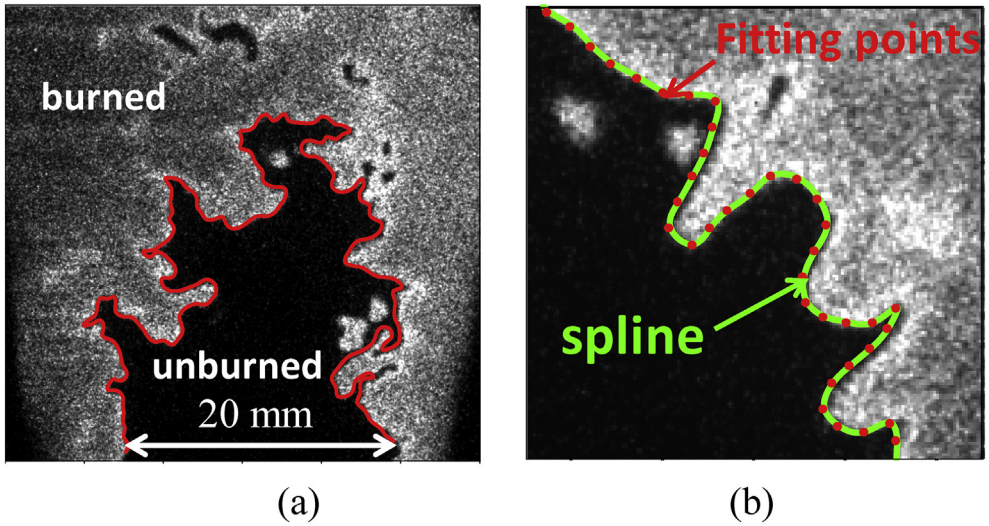

Fig. 12 – Local flame parameter processing (a) flame front extracting (b) fitting the flame with spline.

Fig. 13 plots the effect of hydrogen ratio on PDF distribution of curvature for two turbulence intensities, corresponding to the cases in Fig. 10. Only ZH2 = 0, 0.4 and 0.8 are compared to illuminate the behavior of hydrogen ratio effect due to brevity.

According to Halter et. Al [36], the acceptable resolution should be no more than three times the Kolmogorov length scale. The pixel resolution of the OH-PLIF image is about 0.11 mm/pixel and the smallest Kolmogorov scale is about 0.04 mm. Therefore, the present resolution can be justified to be adequate to capture the curvature of the flame front. The peak of the PDF corresponds to small positive curvatures arising from the large rounded troughs of the flame surface, and the large negative curvatures correspond to the highly pointed crests. The PDF profiles exhibit a slight positive bias for both condition. At $u'/S_L \approx 0.9$, the peak value of PDF decreases and the profile widens encompassing a larger range with increasing hydrogen ratio, indicating that the small scale wrinkled structure on flame front is enhanced, as seen from Fig. 10. For higher values of $u'/S_L \approx 3.0$ (4.9), the peak value of PDF still show a decreasing trend while the hydrogen effect became smaller. Since the scale of the flame largely decreases, we next present the local radius of curvature, which can be considered as a length scale of the flame front [37].

Fig. 14 plots the PDF distribution of the radius of curvature for the two cases discussed above. The positive/negative is consistent with the definition of curvature. The two peaks at both sides indicate there exists a most frequent scale on the flame, which can be viewed as the dominated small scale. In addition, the PDF distribution of radius of curvature shows an obvious bias to positive radius corresponding to the convex structure that is consistent with the distribution of κ. This indicates that the convex structure, which is convex to the unburned mixtures, is always more frequent than that of the concave structure for turbulent premixed flame. It can be seen that this scale decreases and the frequency increases with hydrogen ratio for $u'/S_L \approx 0.9$. This indicates that hydrogen addition increases combustion intensity through increasing

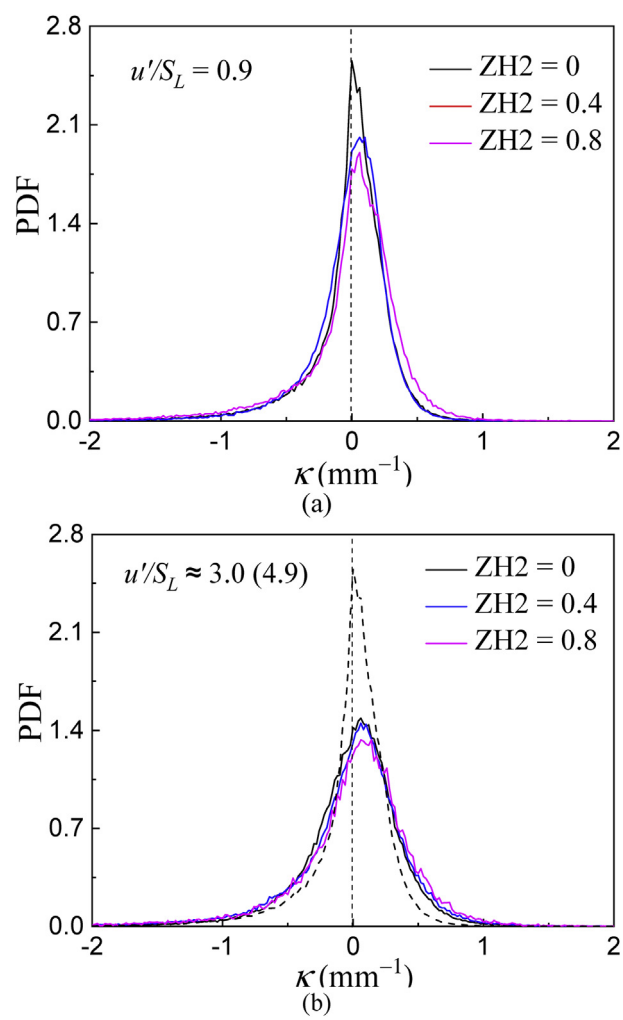

Fig. 13 – PDF distributions of the flame front curvature corresponding to Fig. 10. In figure (b) $u'/S_L \approx 3.0$ for ZH2 = 0 and 0.4, $u'/S_L \approx 4.9$ for ZH2 = 0.8. The dash line represents the data of $u'/S_L \approx 0.9$ for ZH2 = 0. The pixel resolution of the OH-PLIF image is about 0.11 mm/pixel.

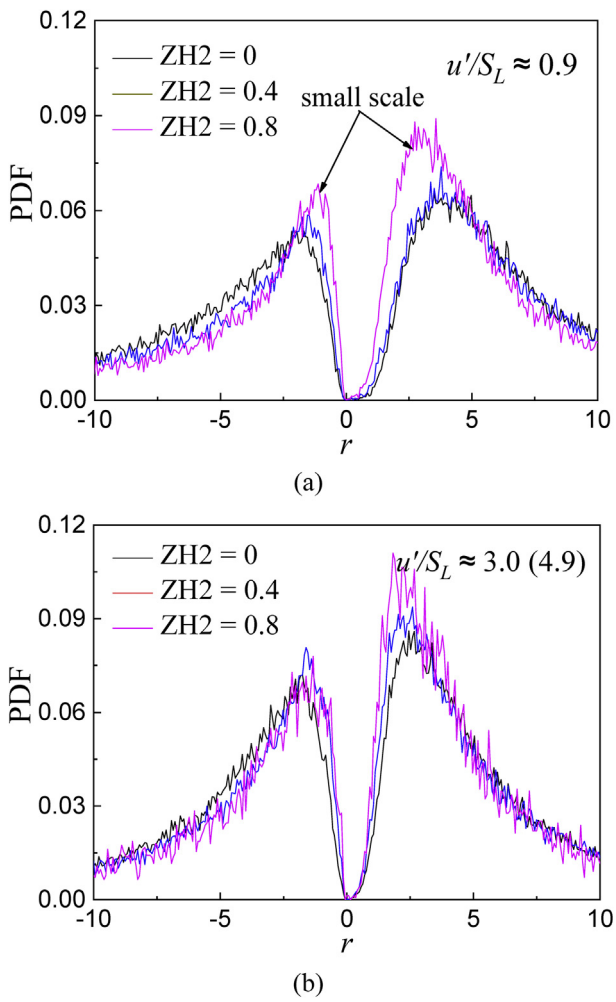

Fig. 14 – PDF distributions of the local radius of curvature corresponding to Fig. 10. In figure (b) $u'/S_L \approx 3.0$ for ZH2 = 0 and 0.4, $u'/S_L \approx 4.9$ for ZH2 = 0.8. The pixel resolution of the OH-PLIF image is about 0.11 mm/pixel.

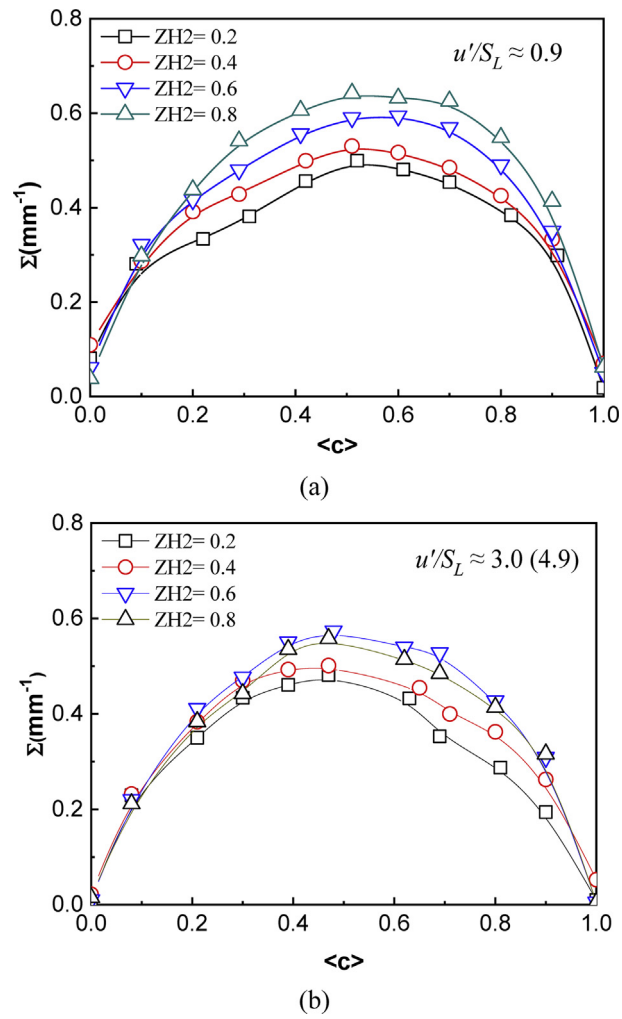

Fig. 15 – Flame surface density versus <c> under different conditions. ($S_{L,0}$≈40 cm/s) (a)P3_D; (b)S2_D.

the flame small scale. While the hydrogen effect behavior is weakened at high intensity, i.e. $u'/S_L \approx 3.0$ (4.9), similar to curvature. This is due to the larger turbulent mixing and turbulent diffusion at larger intensities.

Flame surface density

Flame surface density, defined as flame area in unit volume, quantifies the wrinkles of flame front and can be calculated with the following formula,

$$\sum = \lim_{\Delta x \to 0} \frac{\overline{A_f}}{\Delta x^3} \cong \lim_{\Delta x \to 0} \frac{\overline{L_f}}{\Delta x^2} \tag{3}$$

where $\overline{A_f}$ and $\overline{L_f}$ represent time averaged flame area and flame length in the control volume or control area of size Δx . $\sum$ is also based on the flame front extraction in Fig. 12 and the detailed calculation method can refer to Refs. [16,33].

Fig. 15 shows variations of the $\sum$ with the mean progress variable <c>, corresponding to Fig. 10. At $u'/S_L \approx 0.9$, hydrogen had an evident effect enhancing flame surface density due to the smaller flame front scale as seen in Figs. 10 and 14 (a). In the lower panel of Fig. 10, though smaller scale flamelet elements dominate flame structure and consequently increase the flame surface and turbulent burning velocity, while we found a slightly decreasing trend when ZH2 is beyond 0.6 at $u'/S_L \approx 3.0$ (4.9). This indicates the flame surface density is not directly connecting to the flame front scale. Further studies are needed on the flame surface density behavior at high hydrogen ratio and high turbulence intensities.

Conclusions

Hydrogen, regarded as one of the most promising renewable energy, has a distinguishable effect on the characteristics of turbulent premixed combustion. This work investigated and analyzed the hydrogen effect on flame topology and characteristics of a turbulent Bunsen flame stabilized on a modified multi-plate burner, by using laser diagnostic technique. Turbulent flames of fuel lean and uniform laminar flame speed of

$S_L \approx 40$ cm/s are investigated and compared. The conclusions are summarized as follows.

1. The finer wrinkled structure is not only induced by increasing turbulent intensity u'/S_L, but also there is a significant enhancement due to the increasing hydrogen ratio. When hydrogen ratio is high, more elongated flame folds are formed and small scale structures are generated, which induces flame pockets detaching from the main flame at large turbulence perturbation for lean flames. However, the flame front shows cusp structure with large negative curvature at high hydrogen ratio for flame of $S_L \approx 40$ cm/s
2. Hydrogen addition apparently enhances turbulent burning velocity and the enhancement is more evident for higher intensities. However, S_T/S_L seems to follow the power law relation for lean flames that shows a quadratic relation for flame of $S_L \approx 40$ cm/s.
3. The PDF profile of curvature and the radius of curvature the scale of wrinkled structure is getting smaller with hydrogen ratio. Hydrogen has an evident effect in enhancing flame surface density which may connect to turbulent burning velocity.

Acknowledgements

This study is supported by National Natural Science Foundation of China (No. 51706172, 91841302) and the China Postdoctoral Science Foundation (2017M613130, 2018T111060).

Appendix A. Supplementary data

Supplementary data to this article can be found online at https://doi.org/10.1016/j.ijhydene.2019.10.194.

REFERENCES

[1] Howarth RW, Santoro R, Ingraffea A. Methane and the greenhouse-gas footprint of natural gas from shale formations. Clim Change 2011;106:679.
[2] Pacala S, Socolow R. Stabilization wedges: solving the climate problem for the next 50 Years with current technologies. Science 2004;305:968–72.
[3] Huang ZH, Wang JH, Liu B, Zeng K, Yu JR, Jiang DM. Combustion characteristics of a direct-injection engine fueled with natural gas-hydrogen blends under various injection timings. Energy Fuels 2006;20:1498–504.
[4] Wang JH, Chen H, Liu B, Huang ZH. Study of cycle-by-cycle variations of a spark ignition engine fueled with natural gas-hydrogen blends. Int J Hydrogen Energy 2008;33:4876–83.
[5] Hu EJ, Huang ZH, Liu B, Zheng JJ, Gu XL. Experimental study on combustion characteristics of a spark-ignition engine fueled with natural gas-hydrogen blends combining with EGR. Int J Hydrogen Energy 2009;34:1035–44.
[6] Zeng S, Gu J, Yang S, Zhou H, Qian Y. Comparison of techno-economic performance and environmental impacts between shale gas and coal-based synthetic natural gas (SNG) in China. J Clean Prod 2019;215:544–56.
[7] Huang Z, Zhang Y, Zeng K, Liu B, Wang Q, Jiang D. Measurements of laminar burning velocities for natural gas–hydrogen–air mixtures. Combust Flame 2006;146:302–11.
[8] Wang J, Huang Z, Tang C, Zheng J. Effect of hydrogen addition on early flame growth of lean burn natural gas–air mixtures. Int J Hydrogen Energy 2010;35:7246–52.
[9] Zeng K, Zhang D. Recent progress in alkaline water electrolysis for hydrogen production and applications. Prog Energy Combust Sci 2010;36:307–26.
[10] Boushaki T, Dhué Y, Selle L, Ferret B, Poinsot T. Effects of hydrogen and steam addition on laminar burning velocity of methane–air premixed flame: experimental and numerical analysis. Int J Hydrogen Energy 2012;37:9412–22.
[11] Ma FH, Wang YF, Ding SF, Jiang L. Twenty percent hydrogen-enriched natural gas transient performance research. Int J Hydrogen Energy 2009;34:6523–31.
[12] Hu E, Huang Z, He J, Jin C, Zheng J. Experimental and numerical study on laminar burning characteristics of premixed methane–hydrogen–air flames. Int J Hydrogen Energy 2009;34:4876–88.
[13] Kido H, Nakahara M, Nakashima K, Hashimoto J. Influence of local flame displacement velocity on turbulent burning velocity. Proc Combust Inst 2002;29:1855–61.
[14] Fairweather M, Ormsby MP, Sheppard CGW, Woolley R. Turbulent burning rates of methane and methane-hydrogen mixtures. Combust Flame 2009;156:780–90.
[15] Zhang M, Wang J, Xie Y, Jin W, Wei Z, Huang Z, et al. Flame front structure and burning velocity of turbulent premixed CH4/H2/air flames. Int J Hydrogen Energy 2013;38:11421–8.
[16] Zhang M, Wang J, Xie Y, Wei Z, Jin W, Huang Z, et al. Measurement on instantaneous flame front structure of turbulent premixed CH4/H2/air flames. Exp Therm Fluid Sci 2014;52:288–96.
[17] Wang J, Wei Z, Zhang M, Huang Z. A review of engine application and fundamental study on turbulent premixed combustion of hydrogen enriched natural gas. Sci China Technol Sci 2014;57:445–51.
[18] Peters N. Laminar flamelet concepts in turbulent combustion. Proc Combust Inst 1986;21:1231–50.
[19] Peters N. Turbulent combustion. Cambridge: University Press; 2004.
[20] Driscoll JF. Turbulent premixed combustion: flamelet structure and its effect on turbulent burning velocities. Prog Energy Combust Sci 2008;34:91–134.
[21] Lee GG, Huh KY, Kobayashi H. Measurement and analysis of flame surface density for turbulent premixed combustion on a nozzle-type burner. Combust Flame 2000;122:43–57.
[22] Deschamps BM, Smallwood GJ, Prieur J, Snelling DR, Gülder ÖL. Surface density measurements of turbulent premixed flames in a spark-ignition engine and a bunsen-type burner using planar laser-induced fluorescence. Proc Combust Inst 1996;26:427–35.
[23] Wang J, Zhang M, Huang Z, Kudo T, Kobayashi H. Measurement of the instantaneous flame front structure of syngas turbulent premixed flames at high pressure. Combust Flame 2013;160:2434–41.
[24] Kobayashi H, Otawara Y, Wang J, Matsuno F, Ogami Y, Okuyama M, et al. Turbulent premixed flame characteristics of a CO/H2/O2 mixture highly diluted with CO2 in a high-pressure environment. Proc Combust Inst 2013;34:1437–45.
[25] Chatakonda O, Hawkes ER, Aspden AJ, Kerstein AR, Kolla H, Chen JH. On the fractal characteristics of low Damköhler number flames. Combust Flame 2013;160:2422–33.
[26] Zhang M, Wang J, Wu J, Wei Z, Huang Z, Kobayashi H. Flame front structure of turbulent premixed flames of syngas oxyfuel mixtures. Int J Hydrogen Energy 2014;39:5176–85.

[27] Wang J, Yu Q, Zhang W, Zhang M, Huang Z. Development of a turbulence scale controllable burner and turbulent flame structure analysis. Exp Therm Fluid Sci 2019;109:109898.
[28] Kee RJ, Grcar JF, Smooke MD, Miller JA, Meeks E. A program for modeling steady, laminar, one-dimensional premixed flames. 1985.
[29] Kee RJ, Rupley FM, Meeks E, Miller JA. A fortran chemical kinetics package for the analysis of gas- phase chemical and plasma kinetics. Albuquerque, NM: Sandia National Laboratories; 1993.
[30] Smith GP, Golden DM, Frenklach M, Moriarty NW, Eiteneer B, Goldenberg M, Thomas Bowman C, Hanson RK, Song S, Gardiner Jr WC, Lissianski VV, Qin Z, http://www.me.berkeley.edu/gri_mech/.
[31] Bouvet N, Halter F, Chauveau C, Yoon Y. On the effective Lewis number formulations for lean hydrogen/hydrocarbon/air mixtures. Int J Hydrogen Energy 2013;38:5949–60.
[32] Zhang M, Wang J, Jin W, Huang Z, Kobayashi H, Ma L. Estimation of 3D flame surface density and global fuel consumption rate from 2D PLIF images of turbulent premixed flame. Combust Flame 2015;162:2087–97.
[33] Zhang W, Wang J, Yu Q, Jin W, Zhang M, Huang Z. Investigation of the fuel effects on burning velocity and flame structure of turbulent premixed flames based on leading points concept. Combust Sci Technol 2018:1–23.
[34] Fogla N, Creta F, Matalon M. Effect of folds and pockets on the topology and propagation of premixed turbulent flames. Combust Flame 2015;162:2758–77.
[35] Patyal A, Matalon M. Nonlinear development of hydrodynamically-unstable flames in three-dimensional laminar flows. Combust Flame 2018;195:128–39.
[36] Halter F, Chauveau C, Gokalp I, Veynante D. Analysis of flame surface density measurements in turbulent premixed combustion. Combust Flame 2009;156:657–64.
[37] Wang JH, Matsuno F, Okuyama M, Ogami Y, Kobayashi H, Huang ZH. Flame front characteristics of turbulent premixed flames diluted with CO2 and H2O at high pressure and high temperature. Proc Combust Inst 2013;34:1429–36.